AFRL-AFOSR-VA-TR-2019-0053

Molecular Tuning of Interfacial Electrocatalysis

Yogesh Surendranath
MASSACHUSETTS INSTITUTE OF TECHNOLOGY

01/04/2019
Final Report

Air Force Research Laboratory
AF Office Of Scientific Research (AFOSR)/ RTB2
Arlington, Virginia 22203
Air Force Materiel Command

REPORT DOCUMENTATION PAGE

Form Approved
OMB No. 0704-0188

1. REPORT DATE *(DD-MM-YYYY)*	**2. REPORT TYPE**	**3. DATES COVERED** *(From - To)*
12/26/2018	Final Report	04/01/2015 - 09/30/2018

4. TITLE AND SUBTITLE
Molecular Tuning of Interfacial Electrocatalysis

5a. CONTRACT NUMBER

5b. GRANT NUMBER
FA9550-15-1-0135

5c. PROGRAM ELEMENT NUMBER

6. AUTHOR(S)
Yogesh Surendranath

5d. PROJECT NUMBER

5e. TASK NUMBER

5f. WORK UNIT NUMBER

7. PERFORMING ORGANIZATION NAME(S) AND ADDRESS(ES)
Massachusetts Institute of Technology
77 Massachusetts Avenue, Rm. 18-292
Cambridge, MA 02139

8. PERFORMING ORGANIZATION REPORT NUMBER
N/A

9. SPONSORING/MONITORING AGENCY NAME(S) AND ADDRESS(ES)
N/A

10. SPONSOR/MONITOR'S ACRONYM(S)
N/A

11. SPONSOR/MONITOR'S REPORT NUMBER(S)
N/A

12. DISTRIBUTION/AVAILABILITY STATEMENT
A

13. SUPPLEMENTARY NOTES

14. ABSTRACT

15. SUBJECT TERMS
proton coupled electron transfer; carbon dioxide reduction; in situ vibrational spectroscopy; gold; silver; palladium; copper; electrochemistry; catalysis

16. SECURITY CLASSIFICATION OF:			**17. LIMITATION OF ABSTRACT**	**18. NUMBER OF PAGES**	**19a. NAME OF RESPONSIBLE PERSON**
a. REPORT	**b. ABSTRACT**	**c. THIS PAGE**			Yogesh Surendranath
N/A	N/A	N/A	UU		**19b. TELEPHONE NUMBER** *(Include area code)* 617-253-2664

INSTRUCTIONS FOR COMPLETING SF 298

1. REPORT DATE. Full publication date, including day, month, if available. Must cite at least the year and be Year 2000 compliant, e.g. 30-06-1998; xx-06-1998; xx-xx-1998.

2. REPORT TYPE. State the type of report, such as final, technical, interim, memorandum, master's thesis, progress, quarterly, research, special, group study, etc.

3. DATE COVERED. Indicate the time during which the work was performed and the report was written, e.g., Jun 1997 - Jun 1998; 1-10 Jun 1996; May - Nov 1998; Nov 1998.

4. TITLE. Enter title and subtitle with volume number and part number, if applicable. On classified documents, enter the title classification in parentheses.

5a. CONTRACT NUMBER. Enter all contract numbers as they appear in the report, e.g. F33315-86-C-5169.

5b. GRANT NUMBER. Enter all grant numbers as they appear in the report. e.g. AFOSR-82-1234.

5c. PROGRAM ELEMENT NUMBER. Enter all program element numbers as they appear in the report, e.g. 61101A.

5e. TASK NUMBER. Enter all task numbers as they appear in the report, e.g. 05; RF0330201; T4112.

5f. WORK UNIT NUMBER. Enter all work unit numbers as they appear in the report, e.g. 001; AFAPL30480105.

6. AUTHOR(S). Enter name(s) of person(s) responsible for writing the report, performing the research, or credited with the content of the report. The form of entry is the last name, first name, middle initial, and additional qualifiers separated by commas, e.g. Smith, Richard, J, Jr.

7. PERFORMING ORGANIZATION NAME(S) AND ADDRESS(ES). Self-explanatory.

8. PERFORMING ORGANIZATION REPORT NUMBER. Enter all unique alphanumeric report numbers assigned by the performing organization, e.g. BRL-1234; AFWL-TR-85-4017-Vol-21-PT-2.

9. SPONSORING/MONITORING AGENCY NAME(S) AND ADDRESS(ES). Enter the name and address of the organization(s) financially responsible for and monitoring the work.

10. SPONSOR/MONITOR'S ACRONYM(S). Enter, if available, e.g. BRL, ARDEC, NADC.

11. SPONSOR/MONITOR'S REPORT NUMBER(S). Enter report number as assigned by the sponsoring/ monitoring agency, if available, e.g. BRL-TR-829; -215.

12. DISTRIBUTION/AVAILABILITY STATEMENT. Use agency-mandated availability statements to indicate the public availability or distribution limitations of the report. If additional limitations/ restrictions or special markings are indicated, follow agency authorization procedures, e.g. RD/FRD, PROPIN, ITAR, etc. Include copyright information.

13. SUPPLEMENTARY NOTES. Enter information not included elsewhere such as: prepared in cooperation with; translation of; report supersedes; old edition number, etc.

14. ABSTRACT. A brief (approximately 200 words) factual summary of the most significant information.

15. SUBJECT TERMS. Key words or phrases identifying major concepts in the report.

16. SECURITY CLASSIFICATION. Enter security classification in accordance with security classification regulations, e.g. U, C, S, etc. If this form contains classified information, stamp classification level on the top and bottom of this page.

17. LIMITATION OF ABSTRACT. This block must be completed to assign a distribution limitation to the abstract. Enter UU (Unclassified Unlimited) or SAR (Same as Report). An entry in this block is necessary if the abstract is to be limited.

AFOSR Award #: **FA9550-15-1-0135, Massachusetts Institute of Technology**
Project Title: **Molecular Tuning of Interfacial Electrocatalysis**
PI: **Yogesh Surendranath**
Report Date: **12/25/2018**
Research period covered by the report**: 4/01/2015 – 9/30/2018**

Introduction and Proposed Goals.

This project aims to develop strategies for *promoting and tuning heterogeneous CO_2 reduction catalysis via molecular control of proton transfer at the interface*. As the studies detailed below showcase, we have uncovered the dramatic role of the proton donor in dictating CO_2 reduction selectivity and have begun to control it at the molecular level using designer molecular proton donors.

Investigation CO_2 Reduction on Pure Metal Surfaces

The electrochemical reduction of CO_2 to fuels provides a possible strategy towards the storage of intermittent renewable energy in energy-dense chemical bonds. Relative to other energy conversion reactions such as oxygen reduction reaction, oxygen evolution reaction, and hydrogen evolution reaction, CO_2 reduction (CDR) is particularly sensitive to surface structure and composition of the electrocatalyst because many CDR products are thermodynamically accessible over a narrow potential range. The development of practical CDR catalysts requires control over product selectivity, which can be easily compromised by impurities that interact with or irreversibly alter the surface.

Group 11 metal surfaces are regarded as the most promising heterogeneous catalysts for this reaction because they display low to moderate overpotentials for CO production and can generate higher order products including methane and ethylene. However, these metal surfaces are known to lose their catalytic activity and selectivity for CDR under steady state electrolysis, eroding the efficiency of the overall reaction over time. Despite posing a clear obstacle to practical implementation of CDR technologies, the mechanistic basis for this activity loss remains poorly understood.

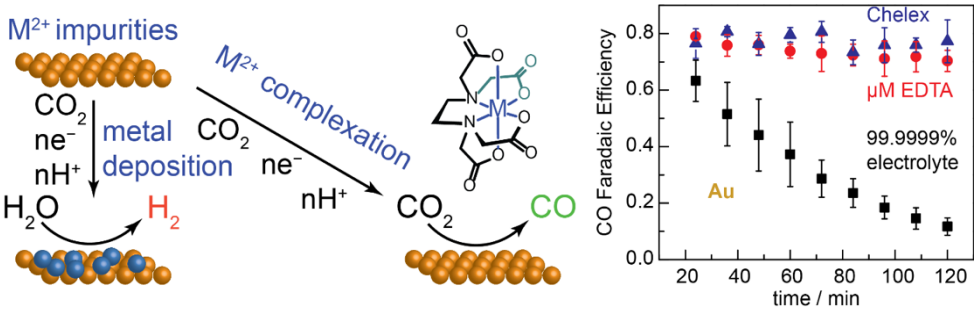

Figure 1. Impurity Ion Coordination Enhances CO_2 Reduction Catalysis. In 99.9999% pure electrolyte, CO production efficiency erodes over the timescale of minutes and begins to favor the competing H_2 evolution. Upon introduction of μM ethylenediaminetetraacetic acid in situ or solid supported imminodiacetate resin ex situ (Chelex), robust CO production efficiency is maintained.

In this work, we show that carbon dioxide reduction are conducted in electrolyte solutions that invariably contain trace concentrations (ppm levels) of metal ion impurities that deposit on the electrode over time, masking the intrinsic activity of the electrode surface and leading to progressive deactivation. We have successfully suppressed electrode deactivation by the chelation of metal impurity ions using ethylenediaminetetraacetic acid in situ or solid supported iminodiacetate resins ex situ. The results show that group 11 carbon dioxide reduction catalyst poisoning operates principally via an impurity-assisted deactivation mechanism. The treatment also allows for reproducible, sustained catalyst activity and selectivity for carbon dioxide reduction on Au, Ag, and Cu electrodes, allowing us to compare experimental results with contemporary theoretical models. Thus, impurity chelation enables detailed mechanistic inquiry into complex multi-electron, multi-proton carbon dioxide reduction reaction on metal surfaces.

Understanding Proton Coupling in CO_2 Reduction

Even in the limit where impurity metal ions are removed from aqueous electrolytes, CO_2 suffers efficiency losses due to the simultaneous reduction of water to H_2. The core problem centers around the lack of understanding how the electrons and protons interact to selectively produce one fuel over another. CDR catalysis at a metal electrode is an ensemble phenomenon that arises from the intrinsic reaction kinetics, proton coupled electron transfer dynamics, and concentration gradients that develop at the interface. Herein, we have use electrochemical kinetics to parse these effects, and we have explicitly accounted for diffusional gradients by comparing experimental data collected on static and rotating electrodes. The data are consistent with a mechanism of CO production involving rate-limiting single electron transfer to CO_2 with concomitant adsorption to surface active sites, followed by rapid one electron, two proton transfer, and CO liberation from the surface. In contrast, the data suggest a H_2 evolution mechanism involving rate-limiting single electron transfer coupled with proton transfer from bicarbonate, hydronium, and/or carbonic acid to form adsorbed H species, followed by rapid one electron, one proton or H recombination reactions.

Thus, we find that for CDR and HER conducted on polycrystalline Au in CO_2-saturated bicarbonate electrolytes: (i) CDR is gated by rate-limiting ET to CO_2, and is not dependent on the proton donor environment; (ii) HER is strongly dependent on the proton donor environment; (iii) the observed transfer coefficients for CDR are higher than those for HER; and (iv) the intrinsic activation-controlled kinetics of CDR and HER are augmented by interfacial diffusional gradients that serve to suppress HER preferentially relative to CDR. These factors determine the critical parameters – proton donor concentration and applied overpotential – that dictate catalyst selectivity. Since CDR is insensitive to the proton donor environment, changes in the interfacial proton activity do not augment the rate of CO production. Furthermore, CO_2 equilibration with bicarbonate is hindered by slow CO_2 hydration kinetics (24 s half-life) preserving a high interfacial CO_2 concentration despite an elevated local pH. These mechanistic insights predict that CDR selectivity can be enhanced over a wider potential range by amplifying proton depletion effects within a porous electrode, a notion supported by our recent studies on ordered porous Au inverse opals (see section below). This work establishes a comprehensive model of the interfacial reactivity of Au under catalytically relevant conditions that highlights the divergent proton-coupling requirements of CDR and HER as key drivers of selectivity in fuel formation.

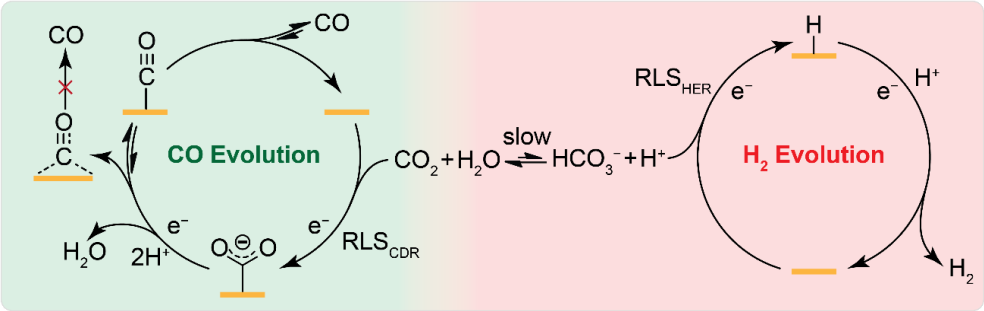

Figure 2 – Predictive mechanistic model constructed for the mechanism for CO (green) and H_2 evolution (red) occurring simultaneously on Au electrocatalyst surfaces during CO_2 reduction.

Mesostructure Induced Selectivity in Au-Catalyzed CO_2 Reduction

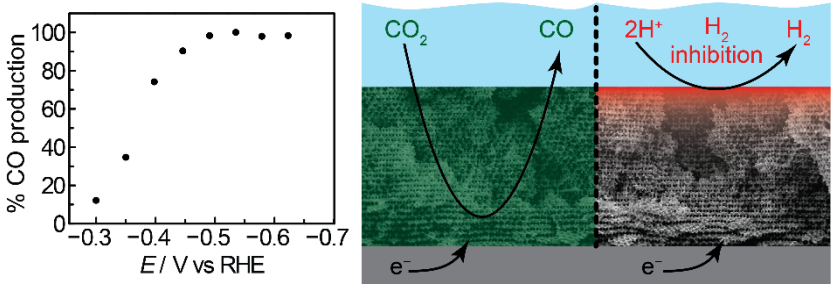

Figure 3 – Mesostructured electrodes locally deplete proton concentration during CDR, leading to HER inhibition. CDR activity remains unperturbed, leading to high CO selectivity.

Recently, numerous nanostructured metals have been shown to catalyze CO_2 reduction with improved selectivity relative to planar polycrystalline foils. For example gold, copper, and lead films prepared by electrochemical reduction of copper, gold, and lead oxides, respectively, display high CDR selectivity at low overpotentials. Likewise, de-

alloyed porous Ag films and carbon-supported Au nanoparticle and nanowire electrodes have been shown to catalyze the reduction of CO_2 to CO with high selectivity. This enhanced selectivity may arise from increases in the specific (surface area normalized) activity for CDR and/or from a decrease in specific activity for HER. For oxide-derived gold, evidence points to both effects, whereas for oxide-derived Cu and Pb, specific HER activity have been shown to diminish more dramatically than CDR activity, giving rise to enhanced selectivity for the latter. In general, selectivity differences have been attributed to the intrinsic selectivity of the active sites in the material. However, observations of thickness-dependent product selectivity for electrodeposited porous copper thin films suggest that mass transport effects may also play a role in determining product selectivity. For example, when considering CO_2 reduction catalyzed by Au, which generates CO and H_2 predominantly, both the desired reaction (eq. 1) and H_2 evolution (eq. 2) consume protons,

$$CO_2 + 2H^+ + 2e^- \rightarrow CO + H_2O \qquad \text{(eq. 1)}$$

$$2H^+ + 2e^- \rightarrow H_2 \qquad \text{(eq. 2)}$$

leading to the formation of a pH gradient at the electrode surface irrespective of the product distribution. However, all high surface area catalysts explored to date exhibit a high degree of disorder in pore size, length, and tortuosity, making it difficult to unambiguously deconvolute surface structure and transport effects.

For reactions in which only a single product is possible, inhibited mass transport in a porous electrode can only serve to reduce specific activity relative to a planar surface. However, the conditions of CO_2 reduction allow for many reactions to take place simultaneously, each of which may be gated by diffusion of a different species. Thus, an appropriately designed mesostructure that takes advantage of the differential transport characteristics of each reaction should enable enhanced selectivity.

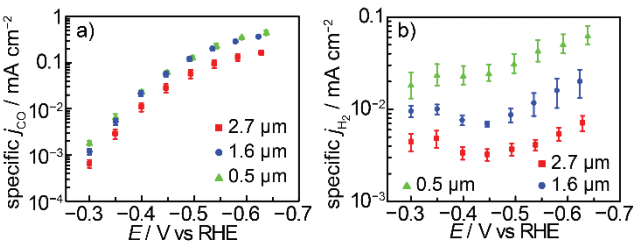

Figure 4 – Specific activity for CO (a) and H_2 (b) evolution for 0.5 (green triangles), 1.6 (blue circles), 2.7 (red squares) µm thick Au-IO samples evaluated in CO_2 saturated 0.1 M $KHCO_3$ electrolyte, pH 6.7. Error bars represent standard deviations of three independently synthesized Au-IO samples for each thickness.

As part of our investigation of mesostructured induced selectivity for CDR, we have discovered that by leveraging mesostructure, rather than surface structure, we are able to modulate CDR selectivity. We synthesized a series of ordered gold inverse opal thin-films (Au-IO) of varying thickness and show that diffusional gradients formed within the porous film dramatically suppress HER specific activity relative to CDR, leading to near quantitative selectivity for CO generation at modest overpotentials. Electrolyses were performed at steady state at a variety of fixed potentials in CO_2 saturated 0.1 M $KHCO_3$ (pH 6.7). The thinnest, 0.5 µm, sample displays the lowest faradaic efficiencies (FE) for CDR at all potentials, whereas the intermediate (1.6 µm) and thick (2.7 µm) electrodes exhibit higher efficiency for CDR. For example, at −0.4 V the 0.5 µm Au-IO films exhibit a faradaic efficiency for CO production of 50% whereas the 2.7 µm and 1.6 µm Au-IO films generate CO with 75% FE. Interestingly, the intermediate and thickest electrodes have similar faradaic efficiency for CDR. For comparison, at −0.4 V, planar polycrystalline electrodes display 50% selectivity for CO production. In concert with the rise of CO FE as the porous film thickness is increased, the HER FE declines. Indeed, within experimental error, CO and H_2 account for all of the current passed in the electrolysis. Taken together, the data suggest that increased electrode porosity serves to improve electrode selectivity for CDR relative to HER.

To isolate the role of the electrolyte in HER and CDR activity, we compared the real surface area normalized specific current density for the production of CO and H_2 at the mesostructured electrodes. Surprisingly, the specific activity for CO production remain the same for all thicknesses, while there is a clear thickness dependent HER suppression. As the sample is made thicker, there is greater suppression of HER, leading to the observed selectivity for CO (Figure 4).

To further explore the origin of the selectivity, we evaluated all samples in CO_2 saturated 0.5 M $KHCO_3$ (pH 7.2). The significantly higher buffer strength serves to diminish large pH gradients that are expected to

form within the pores of Au-IO films. As expected from our hypothesis we observed diminished enhancements in CO production faradiac efficiency as a function of electrolyte composition in this buffering media.

In summary, we have shown that electrode mesostructuring is a powerful tool for tuning the selectivity of CO_2 reduction catalysis regardless of surface structure. Diffusional limitations imposed by a porous electrode serve to inhibit hydrogen evolution while preserving high rates of CO_2 reduction to CO. These results highlight that changes in the observed selective for CDR cannot, a priori, be exclusively attributed to changes in the intrinsic selectivity of surface active sites. Indeed, a complex interplay between surface structure, electrode mesostructure, and the electrolyte composition serve to define the experimental selectivity. The ordered porous environments provided by metal inverse opals make them an ideal platform for deconvoluting these effects, enabling accurate simulations of surface concentration profiles and systematic studies of reaction mechanism.

Mesostructure Induced Selectivity in Ag-Catalyzed CO_2 Reduction

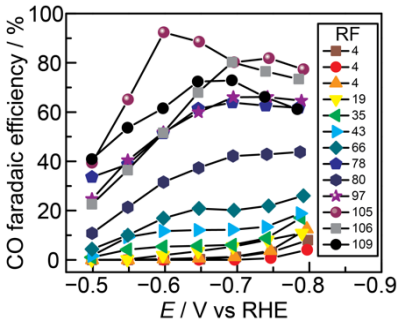

Figure 5 - Faradaic efficiency for CO production as a function of applied potential for Ag films of varying roughness factors (RF). All data were collected in CO_2-saturated 0.1 M $KHCO_3$.

For a simple electrochemical reaction involving a single diffusion species that converts to a single product, transport limitations at an electrode surface can only serve to decrease intrinsic catalytic performance. However, for aqueous CDR catalysis in which multiple reaction partners are involved in multiple concurrent reaction paths, transport limitations can lead to several possible outcomes in terms of overall electrode performance. If the undesired pathway is more sensitive to transport limitations than the desired reaction, electrode selectivity will improve, but the specific activity for the desired reaction will remain unchanged. We have demonstrated this phenomenon for Au-catalyzed CDR in the previous section, for which mesostructuring induces transport limitations that suppress the rate of H_2 evolution but leave the rate of CO production largely unchanged. Likewise, enhanced selectivity on mesostructured oxide-derived Ag surfaces has been attributed, in part, to transport-limitation-induced H_2 suppression. A tantalizing alternative possibility, which is entirely unprecedented, is one in which transport limitations serve to *promote* the desired reaction while *simultaneously suppressing* the undesired reaction. In this limit, the electrode's specific activity, selectivity, and geometric activity would all be enhanced concomitantly. In our exploration of the generality of diffusion effects on other Group 11 catalysts, we synthesized ordered and mesostructured Ag inverse opal (Ag-IO) electrodes, and demonstrated that increasing the thickness of the mesostructure, without changing the surface structure, effects simultaneous *promotion* of CO generation and *suppression* of HER, allowing for dramatic tuning of CO_2-to-fuels selectivity from <5 % to >80 %.

To probe the dependence of CDR selectivity on the mesostructure of the electrode, we compared the performance of a variety of Ag-IO samples of different thickness and roughness factors (RF) as well as nominally planar Ag films (RF = ~4) deposited in the absence of an IO host template. Data were collected as a function of potential from −0.50 V to −0.80 V in CO_2-saturated 0.1 M $KHCO_3$ (pH 6.8) (Figure 5). To effectively compare the data across both planar Ag films and Ag-IO films, the data are color coded by electrode RF. Planar Ag electrodes uniformly display very low selectivity for CO production over the entire range of the potentials explored (Figure 5), with the onset of measureable CO selectivity occurring beyond -0.75 V. In contrast, we observed significantly enhanced faradaic efficiency (FE) for CO production for Ag-IO samples along with a general increase in CO selectivity as the Ag-IO thicknesses and electrode RF values increase. Indeed, for the thickest Ag-IO samples examined (~6.2 μm), which display roughness factors of >100, we observed appreciable CO selectivity at −0.50 V which rises to >80% at −0.70 V. Together the data indicate

that, remarkably, increasing the electrode roughness factor via mesostructuring is sufficient to enhance the CO FE from <5% to >80 %.

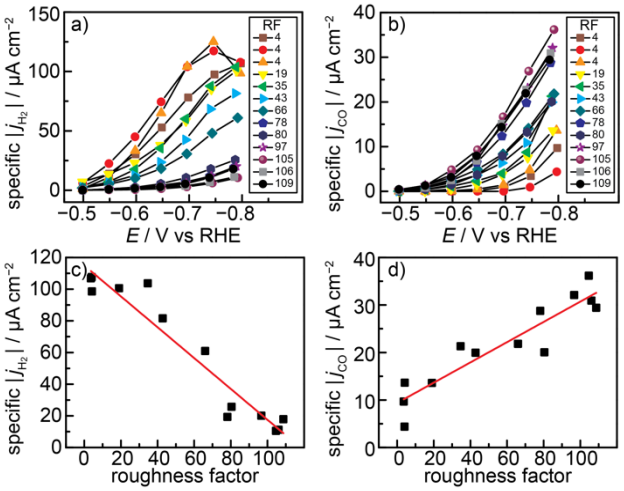

Figure 6 - Specific current density for H_2 (a) and CO (b) evolution as a function of applied potential for Ag films of varying roughness factor (RF). Specific current density at −0.80 V for H_2 (c) and CO (d) evolution as a function of electrode RF. All data were collected in CO_2-saturated 0.1 M $KHCO_3$.

To probe the origin of the enhanced CO selectivity as a function of RF, we compared the specific activity for CO and H_2 production at a variety of potentials for Ag electrodes of varying porosities and thicknesses (Figure 6). Specific current densities (j) were obtained by normalizing the partial currents of H_2 and CO production to the ECSA of each electrode. In CO_2-saturated 0.1 $KHCO_3$ electrolyte, the low RF planar Ag electrodes displayed the highest specific activities for H_2 production over the entire potential range, whereas the thickest Ag-IO samples displayed the lowest j_{H2} values (Figure 6a). Indeed, at −0.8 V, the specific activity for H_2 production declines systematically as a function of electrode RF with a ~10 fold decline over the range of electrode RF values explored here (Figure 6c). These data are in line with our previous observations on Au-IO electrodes suggesting that H_2 suppression is a general phenomenon that arises intrinsically as a consequence of increased electrode mesostructure.

Remarkably, the suppression of H_2 production was not the only source of enhanced overall selectivity. In contrast to the behavior observed for H_2 production, the low RF Ag electrodes displayed the lowest specific activities for CO production over the entire potential range, whereas the thickest Ag-IO samples displayed the highest j_{CO} values (Figure 6b). At −0.8 V, the specific activity for CO production *rises* systematically as a function of electrode RF with a ~3 fold increase over the range of electrode RF values explored here (Figure 6d). Together, the data indicated that there is a synergistic interplay between simultaneous promotion of CO evolution and suppression of H_2 evolution that give rise to the dramatic improvement in overall CDR selectivity. Through these results, we demonstrated that electrode mesostructuring is a powerful general strategy for tuning CDR selectivity *and* activity in the case of Ag, independent of the surface structure and/or active site density of the catalyst.

Tracking the Key CO Intermediate En-Route to High Order Reaction Products

Our understanding of controlled proton flow to the interface allows us to rationally design systems to achieve selective activation of CO_2 over H^+ to form the two-electron reduced CO product. However, higher order product formation requires the further reduction of CO_2 to form desirable species such as ethylene and various alcohols. Metallic Cu has been reported to be the most versatile CO_2-to-fuels catalyst, capable of generating a wide array of value-added products, including methane, ethylene, and ethanol. The rational

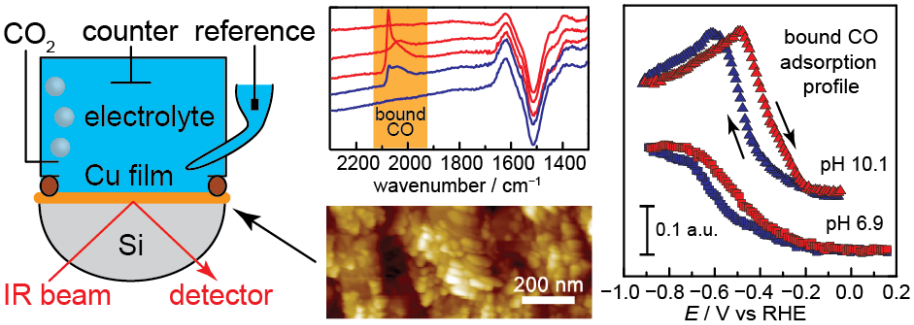

Figure 7: (**left**) *In-situ* spectroelectrochemical cell for surface-enhanced infrared absorption spectroscopy (SEIRAS) studies. (**middle-top**) SEIRA spectra showing the evolution of electrogenerated surface-bound CO on polarized Cu surfaces. (**middle-bottom**) Atomic force microscopy image of Cu films used for SEIRAS. (**right**) pH-dependence of CO adsorption profiles on polarized Cu surfaces during CO_2 reduction.

design of more selective and efficient catalysts requires predictive mechanistic models that explain how Cu catalyzes the kinetically demanding multi-proton and multi-electron conversion of CO_2. Although the mechanistic proposals that have been put forward thus far differ in the assignment of the rate-limiting step for the formation of each product and the surface structures responsible for these rate-limiting steps, in all cases, these models invoke a common intermediate, surface-bound CO, which precedes the formation of all higher order fuels. Therefore, the kinetics and thermodynamics of CO adsorption to Cu is expected to play a central role in determining fuel formation selectivity and efficiency, highlighting the need for direct observation of CO surface binding equilibria under catalytic conditions. In our studies, we synthesize nanostructured Cu films adhered to IR-transparent Si prisms, and we find that these Cu surfaces enhance IR absorption of bound molecules. Using these films as electrodes, we track the dynamics of surface-bound CO in situ under varying (pH, potential, CO concentration) CO_2 reduction conditions *in situ* via surface-enhanced infrared absorption spectroscopy (SEIRAS) for the first time. We compare these spectroscopic results on Cu to those we obtained on Au, a catalyst surface that only produces CO and not higher order fuels.

We show that the adsorption energetics and dynamics of a key intermediate, CO, are extremely different on gold and copper. We discovered two binding modes of CO on Au, linearly bonded and bridge-bonded CO. By tracking the spectroscopic signatures for CO under CO_2 reduction conditions on Au, we discovered that the linearly bonded CO is reversibly bonded to the surface and exists in extremely low surface population, so it can be readily liberated from the surface to form Au's sole product of CO_2 reduction, CO. We found that bridge-bonded CO is irreversibly bonded to the surface to ~20% of the Au sites and acts as kinetically inert spectators.

In contrast to Au, where kinetically competent linearly bonded CO dissociate from the surface, surface-bound CO species, electrogenerated from CO_2, accumulate progressively on the Cu surface. We observe that Cu surfaces bind electrogenerated CO, derived from CO_2, beginning at –0.6 V vs RHE with increasing surface population at more negative potentials. Adsorbed CO is in dynamic equilibrium with dissolved ^{13}CO and exchanges rapidly under catalytic conditions. The CO adsorption profiles are pH independent, but adsorbed CO species undergo a reversible transformation on the surface in modestly alkaline electrolytes. These results explain the general observation that CO reduction is more facile in alkaline electrolytes; a higher CO surface population can be achieved at lower effective overpotential in more alkaline electrolytes. Taken together with Cu's unique ability to mediate higher order fuel synthesis beyond CO, these observations provide insight into the requirements for the accumulation of surface-bound CO species that can be reduced to higher order products beyond CO.

Molecular Control over Interfacial PCET

In addition to structuring Au electrodes to create pH gradients that suppress the production of H_2 and increase selectivity for CDR products, we have demonstrated that the rate of HER can be controlled by careful selection of the proton-donating electrolyte. Heterogeneous HER must proceed through an intermediate consisting of a surface-bound H atom formed during a concerted proton electron transfer (CPET) step. Nearly all previous kinetic studies of HER on Au had been conducted in aqueous acid electrolyte, a medium that presents the surface with the least hindered proton donor, solvated H^+, so very little was known about the sensitivity of interfacial CPET to the structure of the proton donor. However, it has been demonstrated that the molecular nature of the proton donor greatly affects the rate of proton-coupled electron transfer (PCET) steps in both biological and molecular systems. In biological systems, enzymes are able to control selectivity and efficiency by using proton-shuttling residues in the second coordination sphere of metallo-cofactors to modulate the relative rates of different PCET steps. In molecular systems, the proton donor has been shown to dictate product selectivity in CO_2 reduction, and the

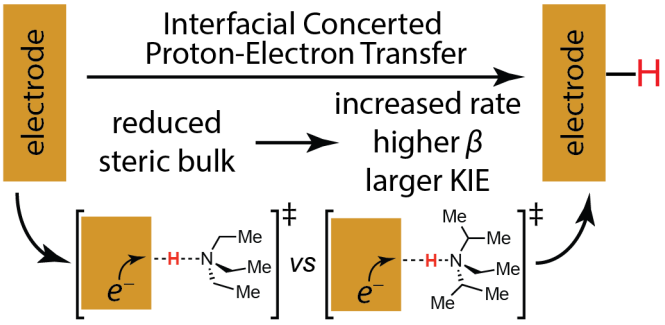

Figure 8 – Depiction of the variation in transition state for interfacial concerted proton electron transfer from proton donors of varying steric bulk.

incorporation of proton relays in ligand frameworks has been shown to improve rates and selectivity in molecular electrocatalysts for H_2 evolution, O_2 reduction, and CO_2 reduction. Our work demonstrated that the proton donor plays a significant role in controlling the rate of interfacial CPET as well.

This study consisted of a detailed mechanistic study of the structural requirements governing interfacial CPET by using the rate of HER catalyzed by polycrystalline Au surfaces as a proxy for the rate of CPET to the surface. Studies in both aqueous and nonaqueous media indicated that Au-catalyzed HER proceeds via a rate-limiting one-electron, one-proton step to form a surface-bound H-atom, consistent with what is reported for Au in aqueous acidic media. Thus, Au-catalyzed HER provided an ideal platform for studying the rate of interfacial CPET because the rate of HER on Au *is* the rate of CPET.

Specifically, we examined the effect of proton donor structure on CPET by comparing the rates of HER catalysis on polycrystalline Au using two trialkylammonium proton donors of identical pK_a, but drastically different steric profiles. We demonstrated that the rate of CPET to a Au electrode in acetonitrile is strongly dependent on the molecular structure of the proton donor. In acetonitrile electrolyte, triethylammonium ($TEAH^+$) displays up to 20-fold faster CPET kinetics than diisopropylethylammonium ($DIPEAH^+$) at all measured potentials. In aqueous electrolyte, this steric constraint is largely lifted, suggesting a key role for water in mediating interfacial PCET. In acetonitrile, $TEAH^+$ also displays a much larger transfer coefficient ($\beta = 0.7$) than $DIPEAH^+$ ($\beta = 0.4$), and $TEAH^+$ displays a potential-dependent H/D kinetic isotope effect that is not observed for $DIPEAH^+$.

These results demonstrate that proton donor structure strongly impacts the free energy landscape for CPET to extended solid surfaces and suggests that suitably designed acids can be used to suppress HER during CDR catalysis, particularly in aprotic electrolytes. Likewise, the results suggest that water's unique role as a promiscuous proton donor must be managed in order to direct CDR selectivity in aqueous electrolytes.

Quantifying Interfacial pH Variation at Molecular Length Scales

Interfacial electrocatalysis is strongly dependent on the proton activity at the electrode surface. Indeed, there is a growing appreciation that the interfacial pH and proton donor environment play a central role in determining the kinetics, thermodynamics, and mechanism of elementary PCET steps, thereby defining the selectivity and efficiency of key interfacial reactions ranging from CO_2 and O_2 reduction to the oxidation of small molecule fuels such as MeOH and HCO_2H. Consequently, knowledge of the pH at the electrode surface and its variation under electrochemical polarization is an essential prerequisite for achieving molecular-level understanding of interfacial reactivity and catalysis.

Depending on the reaction conditions and electrode morphology, the pH gradient can extend 1-10 μm from the electrode surface into the reaction diffusion zone. Variations in the pH in the reaction diffusion zone have been quantified using a variety of spectroscopic and electrometric methods. However, heterogeneous electrocatalytic reactions proceed via inner-sphere mechanisms that require the binding of small-molecule substrates to the electrode surface. Thus, the pH within molecular length scales of the surface, rather than the value remote from the electrode in the reaction diffusion layer, is critical for defining the free-energy landscape for catalysis. Despite its central importance, direct measurements of the pH variation in this narrow region near the electrochemical double layer (< 1 nm from the electrode surface) are, to the best of our knowledge, unprecedented.

Herein, we establish the first localized measurements of pH variation within the critical double layer region during electrocatalysis by utilizing a concurrent, surface-catalyzed, non-faradaic probe reaction that displays pH-dependent selectivity. Specifically, using the hydrogen oxidation reaction (HOR) on Pt as a model system, we exploit the pH-dependent bifurcation between hydrogenation and hydrogenolysis of a *cis-2-butene-1,4-diol* probe molecule to measure the pH variation <1 nm from the catalyst surface over a diverse range of current densities and buffer compositions (Figure 9).

First, the aqueous pH dependence of the Pt-catalyzed reaction of H_2 with *cis-2-butene-1,4-diol* was measured in the absence of current flow to determine the inherent pH sensitivity of the non-faradaic probe reaction. Using commercially available fuel cell electrodes (Pt/C GDE), which contains Pt nanoparticles embedded in microporous carbon layers; we examined the reaction at the open circuit potential (OCP) under a variety of bulk pH and electrolyte conditions. In all cases, the reaction proceeds cleanly to generate a

mixture of *1,4-butanediol* (A) and *n-butanol* (B). The ratio of these two products is strongly dependent on the bulk pH. Importantly, for these calibration experiments, the electrode was held at the OCP (close to RHE in all cases), ensuring the complete absence of net current flow and, thus, no proton influx/efflux from the surface.

The kinetic data provide information about the mechanism of product bifurcation. The rate of *1,4-butanediol* formation increases as the pH rises, whereas the rate of *n-butanol* formation increases as the pH declines. Importantly, over the entire pH range explored, we observe that the total conversion rate remains constant, despite large variations in the product selectivity. From this, we propose that, following these adsorption events, rate-limiting surface recombination of H and the substrate generates a common surface-bound intermediate, that bifurcates to A and B via pH dependent pathways. This ensures that the reaction probe is uniquely sensitive to the local pH environment within 1-2 C–C/C–O bond lengths of the Pt surface.

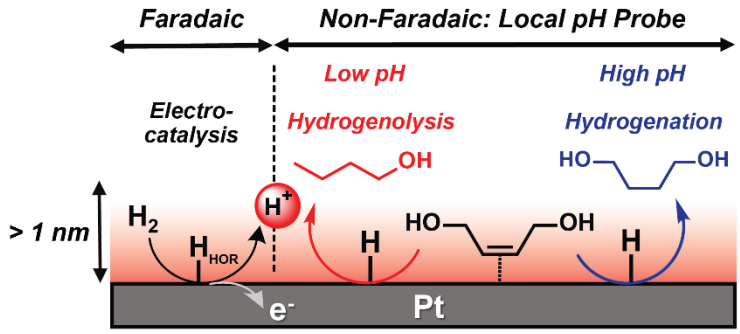

Figure 9: Highly localized measurements of interfacial pH near the double layer region during HOR electrocatalysis (left) are enabled by a concurrent pH-sensitive non-faradaic reaction (right): Pt catalysed H_2 addition to cis-2-butene-1,4-diol to produce 1,4-butanediol and n-butanol

We next examined the dependence of product selectivity on concurrent HOR electrocatalysis as a function of the electrolyte environment. In 50 mM phosphate electrolyte, pH 6.8, varying the HOR current densities from 0.0 to 4.6 mA cm^{-2}, gave rise to a dramatic increase in selectivity for B from 21 to 63%. When the buffer strength was increased to 100 mM phosphate, the same range of HOR current densities led to an attenuated increase in selectivity for B from 20 to 38%. Exchanging the electrolyte for citrate also attenuated the change in product selectivity at a given current density. In 50 mM citrate electrolyte, the same range of current densities gave rise to a change in selectivity for B from 37% to 50%, whereas in 100 mM citrate, the selectivity change was further attenuated with a variation from 30% to 41% over the same current range. These observations establish that concurrent HOR serves to increase the selectivity towards B in all cases and that the magnitude of this change is positively correlated to the current density and is also dependent on the buffer type and concentration.

Based on the analysis above, the product selectivity for the non-faradaic reaction provides a measure of the interfacial pH near electrochemical double layer under concurrent HOR catalysis. With the pH dependence of product selectivity measured at OCP, we used the product selectivities measured during concurrent HOR to estimate the change in interfacial pH relative to the bulk value (ΔpH). Remarkably, at a modest current density of 4.6 mA cm^{-2} in 50 mM phosphate electrolyte, we estimate an interfacial pH of 3.6, 3.2 units lower than the bulk value of 6.8. Unsurprisingly, ΔpH is negative in all cases because HOR generates H^+ at the interface and, as expected, the ΔpH becomes more negative as the HOR current density increases. Interestingly, the 50 and 100 mM phosphate buffers display a more negative ΔpH than 50 or 100 mM citrate buffers. These trends are consistent with the enhanced buffer capacity of citrate relative to phosphate below pH ~6.25 resulting from citrate's closely-spaced pK_a values and its higher buffering capacity in that pH region.

Competition between H and CO for Active Sites Governs Copper Mediated Electrosynthesis of Hydrocarbon Fuels

In the electrochemical reduction of CO_2 on copper, it is widely accepted that surface-bound carbon monoxide (CO_{ads}) serves as the key intermediate en route to hydrocarbons and oxygenates. Synthesis of these products will by necessity require C-H and C-C bond formation events. However, little is understood about the processes taking place at the electrode surface. Specifically, in forming a bond, two distinct surface-reaction mechanisms can be in play: surface-bound species can react with each other in what the heterogeneous catalysis field calls a "Langmuir-Hinshelwood" (LH) step or a surface-bound species can react with a species in solution in what is termed an "Eley-Rideal" (ER) step. Insight into this mechanistic distinction is essential for the design of efficient CO_2 reduction catalysts. For example, in an ER mechanism leading to methane, simply increasing the surface concentration of CO at the expense of H adsorption is sufficient to promote higher-order product formation relative to H_2 evolution. In contrast, for an LH mechanism, both H *and* CO affinity must be simultaneously optimized and the product distribution will invariably show a complex dependence on their surface population and competition for sites, as well as their reaction rates, requiring more nuanced catalyst design. Despite the critical role of C-H and C-C bond formation steps in the production of higher order fuels and chemicals, there is no clear experimental evidence to parse these mechanistic regimes, impeding the systematic development of selective CO_2 to fuels catalysts. Indeed, investigations along these lines have so far been hampered by the low solubility of CO in aqueous electrolytes (1.1 mM), which severely restricts the concentration range over which activation-controlled CO reduction kinetics can be probed. Furthermore, the mechanistic regimes become distinguishable at near saturation CO coverage, therefore requiring an experimental approach that fosters strong CO binding to the Cu surface. We overcame these challenges by examining the electrochemical reduction of CO on polycrystalline Cu in ethanol at – 35℃ using 0.1 M LiTFSI as supporting electrolyte. These conditions are essential to afford high CO solubility, long term catalyst stability, and promote CO adsorption. Exploiting these advantages, we successfully determine the CO-dependent reaction kinetics for H_2, ethylene, and methane and assemble a mechanistic model providing unprecedented insight into the elementary reaction steps.

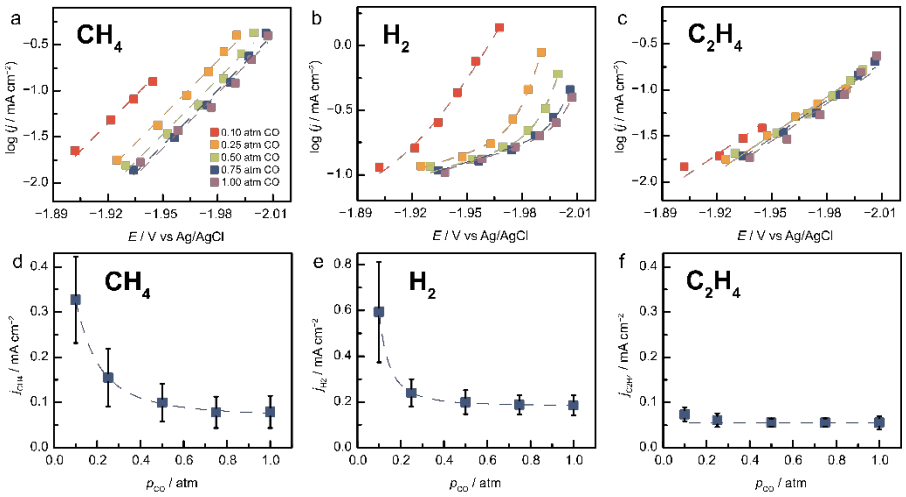

Figure 10: Tafel plots of the partial current density of methane production (a), hydrogen evolution (b) and ethylene production (c) under varying partial pressures of carbon monoxide in 0.1M LiTFSI / EtOH at -35℃. Dashed lines correspond to fitted data. Partial current densities vs CO pressure at -1.96 V from methane (d), hydrogen (e) and ethylene (f). Data correspond to the average and standard deviation of four independent measurements. Dotted lines in d, e, and f serve as guides to the eye.

Methane production is dramatically suppressed upon increasing CO partial pressure, with the Tafel curves shifting progressively to higher overpotentials (Figure 10a) corresponding to a strong decline in j_{CH4} at constant bias (Figure 10d). The data reveal a reaction order of -0.7 despite the fact that CO is a reactant for methane production. Hydrogen evolution is equally suppressed by increasing concentrations of CO (Figure 10b and e). Together, these data yield a clear mechanistic picture, wherein CO and H intermediates compete surface sites (Figure 11). In our conditions, the surface is highly saturated with CO, hydrogen being the minority species. The reaction order of -0.7 and Tafel slope of 55 mV dec^{-1} indicate that Methane production takes place through the Langmuir-Hinshelwood reaction between surface-bound CO and H. As the concentration of CO increases, less sites are available for hydrogen to bind, thereby explaining the decreasing formation rate of methane with increasing CO partial pressure. Similarly, the low Tafel slope of hydrogen evolution (22 mV dec^{-1}), together with its reaction order of -2.1 indicates that it takes place through the Langmuir-Hinshelwood reaction of two surface-bound hydrogen species, the surface concentration of which decreases with increasing CO partial pressure. Ethylene, on the other hand, showed minimal dependence on the partial pressure of CO (Figure 10 c and f) and its Tafel slope indicates a rate-limiting electron transfer. Previous literature suggested ethylene production to take place through an electron-mediated rate-limiting coupling of two surface-bound CO intermediates. Our data is consistent with this picture. Since the surface is nearly saturated with CO, further increases in CO partial pressure will not meaningfully modify the surface concentration of CO relative to its initial value, hence leading to an unchanged rate of ethylene production. As a conclusion, ethylene, too, is produced through a Langmuir-Hinshelwood step.

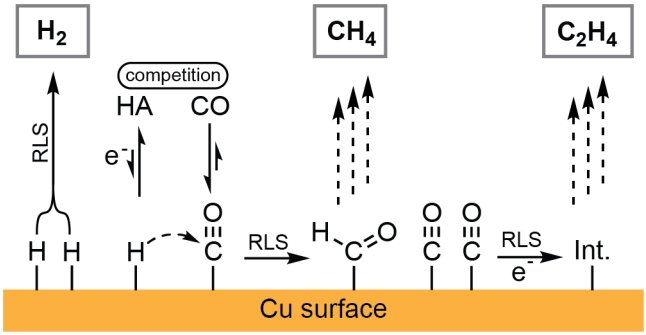

Figure 11: Proposed mechanistic model for methane, ethylene and hydrogen production during the

Publications generated over the grant period:

(9) Schreier, M.; Yoon, Y.; Jackson, M. N.; **Surendranath, Y.** *Angew. Chem. Int. Ed.* **2018**, *57*, 10221–10225.
"Competition Between H and CO for Active Sites Governs Cu Mediated Electrosynthesis of Hydrocarbon Fuels"

(8) Ryu, J.; Wuttig, A.; **Surendranath, Y.** *Angew. Chem. Int. Ed.* **2018**, *57*, 9300–9304.
"Quantification of Interfacial pH Variation at Molecular Length Scales Using a Concurrent Non-Faradaic Reaction"

(7) Wuttig, A.; Yoon, Y.; Ryu, J.; Surendranath, Y. *J. Am. Chem. Soc.* **2017**, *139*, 17109–17113.
"Bicarbonate is Not a General Acid in Au-Catalyzed CO_2 Electroreduction"

(6) Yoon, Y.; Hall, A. S.; Surendranath, Y. *Angew. Chem. Int. Ed.* **2016**, *55*, 15282–15286.
"Tuning of Silver Catalyst Mesostructure Promotes Selective Carbon Dioxide Conversion into Fuels"

(5) Wuttig, A.; Can, L.; Peng, Q.; Yaguchi, M.; Motobayashi, K.; Osawa, M.; Surendranath, Y. *ACS Cent. Sci.* **2016**, *2*, 522–528.
"Tracking a Common Surface-Bound Intermediate during CO_2-to-Fuels Catalysis"

(4) Wuttig, A.; Yaguchi, M.; Motobayashi, K.; Osawa, M.; Surendranath, Y. *Proc. Natl. Acad. Sci. U. S. A.* **2016**, *113,* E4585–E4593.
"Inhibited Proton Transfer Enhances Au-Catalyzed CO_2-to-Fuels Selectivity."

(3) Jackson, M. N.; Surendranath, Y. *J. Am. Chem. Soc.* **2016**, *138*, 3228–3234.
"Donor-Dependent Kinetics of Interfacial Proton-Coupled Electron Transfer."

(2) Hall, A. S.; Yoon, Y.; Wuttig, A.; Surendranath, Y. *J. Am. Chem. Soc.* **2015**, *137*, 14834–14837.
"Mesostructure-Induced Selectivity in CO_2 Reduction Catalysis."

(1) Wuttig, A.; Surendranath, Y. *ACS Catal.* **2015**, *5,* 4479–4484.
"Impurity Ion Complexation Enhances Carbon Dioxide Reduction Catalysis."

Project personnel and percent funding from award:

Anna Wuttig, Graduate Student, 100%
Youngmin Yoon, Graduate Student, 100%

Concluding Remarks.

The research carried out as part of this grant provided a substantially improved understanding proton transfer dynamics and the molecular-level mechanisms that govern selective CO_2 reduction on metal surfaces. Our mechanistic insights establish the following: (1) CO_2 reduction to CO on Au and Ag proceeds through rate-limiting electrosorption of CO_2 that is decoupled from proton transfer (2) unlike CO production, H_2 production is highly sensitive to the local proton donor environment and the molecular structure of the proton donor (3) the further reduction of CO on Cu surfaces is governed by a central competition between adsorbed H and CO species. In pursuit of these mechanistic insights, we have developed robust methods for purifying electrolytes for highly reproducible studies of CO_2 reduction catalysis and we have developed non-faradaic reaction probe of the local pH environment at the catalyst surfaces. Finally, we have deployed this mechanistic understand to rationally design catalysts with tunable selectivity for CO production on both Au and Ag surfaces. In summary, the work demonstrates that molecular control of the electrochemical CO_2 reduction catalysis can be achieved by molecular control of the proton donor involved in critical PCET reaction steps.